Journal of Applied Polymer Science

Synthesis and Characterization of Organic/Inorganic Epoxy Nanocomposites from Poly(aminopropyl/phenyl)silsesquioxanes

Chavakorn Samthong,[1] Richard M. Laine,[2,3] Anongnat Somwangthanaroj[1]

[1]Department of Chemical Engineering, Faculty of Engineering, Chulalongkorn University, Thailand 10330
[2]Department of Materials Science and Engineering, University of Michigan, Ann Arbor, Michigan 48109
[3]Macromolecular Science and Engineering, University of Michigan, Ann Arbor, Michigan 48109
Correspondence to: A. Somwangthanaroj (E-mail: anongnat.s@chula.ac.th)

ABSTRACT: Organic/inorganic epoxy nanocomposites containing diglycidyl ether of bisphenol A (DGEBA), 4-methylhexahydrophthalic anhydride (MHHPA) and poly(aminopropyl/phenyl) silsesquioxanes (PAPPS) were prepared and characterized. PAPPS were synthesized via fluoride-catalyzed cage formation from random-structured poly(phenyl)silsesquioxane (PPS) and 3-aminopropyltriethoxysilane (APTES) in tetrahydrofuran (THF) using tetrabutylammonium fluoride (TBAF) catalyst containing substantial water. The PPS/APTES stoichiometric ratios were varied. The FTIR, ^{1}H, solid-state ^{29}Si-NMR studies show that PAPPS probably consists of cages, partial cages, and some linear structures containing phenyl and aminopropyl functional groups. The amine content was determined by back titration and elemental analysis. In comparison with neat epoxy, incorporation of these materials can improve the resultant thermal stabilities, raise glass transition temperatures (T_gs), and reduce coefficients of thermal expansion (CTEs) of epoxy nanocomposites as confirmed by TG/DTA, DMA and TMA tests, respectively. © 2012 Wiley Periodicals, Inc. J. Appl. Polym. Sci. 128: 3601–3608, 2013

KEYWORDS: composites; thermal properties; thermosets

Received 17 June 2012; accepted 10 September 2012; published online 30 September 2012
DOI: 10.1002/app.38575

INTRODUCTION

There is recent intense interest in the development of silsesquioxane (SQ) based materials based on their 3D nature, their ability to offer a very high degree of functionalization, their ease of synthesis and typically high thermal stability. This is evidenced by the fact that there are now some 17 reviews on SQs and the related Q silicates.[1–17] These references describe their potential application in a broad range of areas from biomedical, to organic light emitting diodes, to nanocomposites.

In our own efforts, we have described their utility in formulating nanocomposites that offer control of coefficients of thermal expansion in epoxy resins from 23 to 230 ppm/°C, and as O_2 barrier materials, as recently summarized.[9] In this work, we used primarily $[NH_2C_6H_4SiO_{1.5}]_8$ as the curing agent varying only the types of epoxy compounds used. Most recently, we discovered a method of using F^- catalysis to form T_{10} and T_{12} mixed $[NH_2C_6H_4SiO_{1.5}]_{2.x}[C_6H_5SiO_{1.5}]_{10/12-2.x}$ SQ systems[18] with the objective of controlling the degree of crosslinking such that it is now possible to produce soluble, processable epoxy resins.

In this work, we discuss several new firsts. These include the first example of the use of F^- catalysis to introduce aminopropyl moieties directly into T_{10} and T_{12} phenylSQs. Second the first example of the use of a monomer, aminopropyltrialkoxysilane, as a reactant in the formation of T_{10} and T_{12} cages. Finally, we provide the first examples of the use of aminopropyl functionalized T_{10} and T_{12} cages to form epoxy resins. The objective here is to provide general methods for the use of aminopropyl functionality to control resin properties with the goal of greatly expanding the utility of SQ systems in diverse epoxy resin applications.

The incorporation of organic/inorganic silsesquioxanes (SQs) into polymer matrices has been extensively investigated to improve nanocomposites properties due to the intrinsic properties of SQs including nanometer dimensions, low densities, excellent heat, and fire-resistant properties as well as the ability to tailor the types and amounts of functional groups. SQs generally consist of silicon-oxygen cores with $(SiO_{1.5})_n$ abbreviated T_n, where $n = 6$, 8, 10, 12 along with pendant organic substituents (R) such as phenyl,[19] vinyl,[20] amine,[21–25] epoxy,[26–29] and arylhalide[30,31] depending on the final required chemical structure and target properties required of the specific application.

The chemical structures of SQ cores include random, partial cage, and cage structures.[2] SQs are an interesting class of organic/inorganic compounds that have been used as a nanobuilding

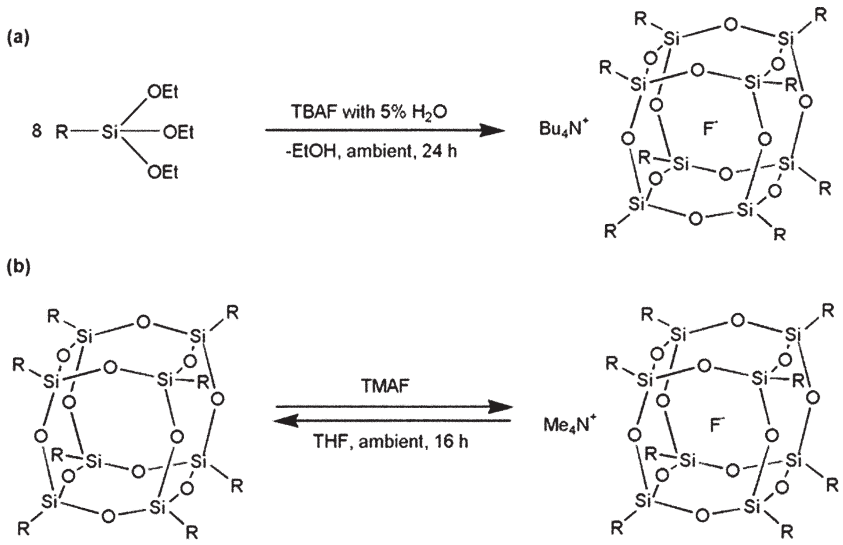

Scheme 1. The fluoride-encapsulation obtained with the use of base catalysts containing fluoride ion from (a) triethoxysilane, and (b) T_8 cages.

blocks owing to their high 3D symmetry, in particular octaSQ (T_8), as well as well-defined architectures. Conversely, polymeric SQs are less useful because the chemical structures are difficult to characterize; however, they offer potential to be applied for use in the preparation of nanocomposites in lieu of particulates such as silica without decreasing the nanocomposite thermomechanical properties significantly.[21]

Acid-catalyzed hydrolysis provides small amounts of T_8 cages,[32,33] whereas base-catalyzed reaction increases the yields of desired products. Kim et al.[23] prepared octa(phenyl)SQ (OPS) with 90% yields from phenyltriethoxysilane in ethanol under reflux condition using KOH as a base. Among various base catalysts, those containing a fluoride ion such as tetrabutylammonium fluoride (TBAF)[34,35] and potassium fluoride (KF),[36] have been widely used for fluoride-catalyzed hydrolytic condensation to prepare SQ cages in reasonable yields.

Bassindale et al.[37] provided evidence for the encapsulation of a fluoride ion in the center of T_8 during the hydrolytic condensation process catalyzed by TBAF containing substantial quantities of water (Scheme 1a) indicated by single-crystal X-ray crystallography and $^{19}F/^{29}Si$-NMR spectroscopy. Bowers et al.[38] prepared a series of fluoride-encapsulated SQ compounds from the reaction between T_8 and tetramethylammonium fluoride (TMAF) in wet tetrahydrofuran (THF) (Scheme 1b). Additionally, the T_8 cages containing an entrapped fluoride ion are obtained in good to excellent yields if R is an electron-withdrawing substituent, e.g., aryl, vinyl, and styrenyl. It was also found that the fluoride ion of TBAF is an important nucleophilic catalyst in cage rearrangements of two random-structured SQs having distinct functional groups at room temperature to produce a novel T_8, T_{10}, and T_{12} cages with di- and trifunctional groups at the vertices.[18,39,40]

Here, our attempt is to synthesize poly(aminopropyl/phenyl)SQs (PAPPS) structures consisting of SQ cores surface functionalized with phenyl and aminopropyl groups, produced via fluoride-promoted rearrangement between poly(phenyl)SQ (PPS) and 3-aminopropyltriethoxysilane (APTES) in THF using TBAF catalyst under water scarce conditions. The PPS/APTES stoichiometric molar ratios were varied between 1:1.5 (PAPPS1) and 1:5.0 (PAPPS2). These materials served as organic/inorganic building blocks to improve the thermomechanical properties of epoxy nanocomposites. The chemical structure of synthesized products and properties of epoxy nanocomposites were characterized by standard tests.

MATERIALS AND METHODS

Materials

Poly(phenyl)SQ (PPS) is a by-product from hydrolytic condensation of phenyltriethoxysilane.[41] 3-aminopropyltriethoxysilane (APTES, 97%), tetrabutylammonium fluoride (1.0 *M* TBAF solution in THF; water ca. 5% wt), tetrahydrofuran, hexane, calcium chloride, diglycidyl ether of bisphenol A (DGEBA) (DER 331, MW 372), 4-methylhexahydrophthalic anhydride (MHHPA, 96%), and 2,4,6-tris(dimethylaminomethyl) phenol (95%) were purchased from Aldrich and used as received without further purification.

Analytical Methods

Fourier Transform Infrared Spectroscopy. Diffuse reflectance Fourier transform IR spectra (DRIFTS) were conducted on a Mattson Galaxy Series FTIR 3000 spectrometer (Mattson Instruments). Optical-grade, random cuttings of crystalline potassium bromide (KBr, International Crystal Laboratories, Garfield, NJ) were used as a background. The analysis sample (5 mg) and KBr crystal (400 mg) were ground together using an alumina mortar and pestle. The ground powder was loaded into the sample holder and leveled off with a glass plate to a smooth surface. The holder was placed in a chamber, and the spectrum was collected under the continuous flow of dry N_2 in a range of 4000–400 cm^{-1} with a resolution of ± 4.0 cm^{-1}.

NMR Analyses. ^1H-NMR data were done in acetone-d_6 (2.05 ppm) and recorded on a Varian INOVA spectrometer at 400 MHz using a 6000 Hz spectral width, a relaxation delay of 3.5 s, 30 k data points, a pulse width of 38°, and tetramethylsilane (TMS,

0.00 ppm) as the internal reference. Solid-state ^{29}Si NMR data were recorded on a Varian INOVA spectrometer at 500 MHz with the frequency of 99.36 MHz, a 20-s pulse delay, a 2-ms contact time and a spinning speed of 5 kHz.

Gel Permeation Chromatography. GPC analyses were performed on a Waters 440 system equipped with Waters Styragel columns (7.8 × 300, HT 0.5, 2, 3, 4) with refractive index detection using a Waters refractometer. THF was used as an eluent, at a flow rate of 1.0 mL/min. The system was calibrated using polystyrene standards and toluene as a reference.

Elemental Analyses

Elemental analyses were run on a CHNS/O Analyzer (Perkin Elmer PE2400 SeriesII, USA). Powder samples (1.5–2.0 mg) loaded into tin vials were combusted at 1000°C in a stream of high-purity oxygen using helium as a carrier gas. Acetanilide was used as a reference standard. Gaseous products were chromatographically separated by frontal analysis and quantitatively detected using a thermal conductivity detector.

Back Titration. The content of amino groups on the synthesized products was quantitatively determined by back titration.[42,43] A typical example is as follows: 0.20 g of PAPPS1 (or PAPPS2) was treated with 20 mL of 0.012 *M* HCl aqueous solution in a 100-mL flask, and the mixture was stirred over 3 h with a magnetic stirrer at room temperature. The reaction mixture was filtered and the filtrate was titrated with of 0.01 *M* NaOH aqueous solution using phenolphthalein as a pH indicator.

Thermogravimetric/Differential Thermal Analysis. Thermal stabilities of PAPPS1, PAPPS2, and epoxy nanocomposites were measured using a 2960 simultaneous DTA-TGA instrument (TA instruments, New Castle, DE). Samples (10–15 mg) were loaded in ceramic pans and the temperature was ramped at 10°C/min to 1000°C under two atmospheres, air and N_2, at flow rate of 100 mL/min.

Dynamic Mechanical Analysis. DMA shows the properties obtained from the dynamic mechanical analysis, the storage modulus (E'), loss modulus (E'') and loss tangent (tan δ). DMA measurements were performed using a dynamic mechanical analyzer (Perkin Elmer, Pyris Diamond, USA). The cured samples were polished to 10 × 2 × 50 mm^3 and mounted on a single cantilever clamp. The thermomechanical properties were measured at a heating rate of 5°C/min from 30 to 150°C under a nitrogen atmosphere using bending mode at a frequency of 1.0 Hz.

Thermomechanical Analysis. TMA is used to measure the coefficient of thermal expansion (CTE) of epoxy nanocomposites while it is subjected to heat. TMA results were recorded using a Perkin Elmer, Pyris Diamond Thermomechanical analyzer, USA, in expansion mode. Samples were polished to give 5 × 5 × 2–3 mm^3 specimens, placed under a quartz probe and heated in a flowing N_2 from 30 to 150°C at a heating rate of 5°C/min.

Synthesis of Poly(aminopropyl/phenyl)SQs

For the synthesis of PAPPS1 (PPS:APTES 1:1.5), PPS (2.00 g) was dissolved in THF (40 mL) with mechanical stirring in a round-bottom flask for 30 min. Next, TBAF (0.14 mL, 0.14 mmol), distilled water (0.16 mL, 8.70 mmol) and APTES (0.52 mL, 2.90 mmol) were added via syringe, and the reaction was carried out at room temperature for 4 days. After the reaction was complete, the clear solution at the top of the reaction mixture was transferred into a 50-mL round-bottom flask containing $CaCl_2$ (5.0 g, 45.0 mmol). The reaction mixture was stirred for 2 h in order to kill the remaining fluoride ions, forming an insoluble CaF_2 solid. The reaction mixture was filtered and the filtrate was vacuum dried. Then, it was redissolved in 5 mL of THF, precipitated into 150 mL of cold hexane, filtered, and a residue was vacuum dried until constant weight was achieved. The white powder was collected to give a yield of 72% with respect to an initial mass of starting PPS.

For the synthesis of PAPPS2 (PPS:APTES 1:5.0), the reaction condition and work-up procedure were similar to the synthesis of PAPPS1with slight difference in mass of starting reactants. PPS (2.00 g), TBAF (0.14 mL, 0.14 mmol), distilled water (0.52 mL, 29.03 mmol) and APTES (1.74 mL, 9.68 mmol) were used instead. The white powder was collected to give a yield of 67% with respect to an initial mass of starting PPS.

Preparation of Epoxy Nanocomposites

Because the synthesized PAPPS1 (or PAPPS2) was hardly dispersed in DGEBA, it was first dissolved in THF (3 mL) and stirred until the solution became clear. The requisite amount of DGEBA was then added and the mixture stirred to give a pale yellow transparent solution. THF was removed slowly in a vacuum oven at 50°C for 12 h. MHHPA and the catalyst, 2,4,6-tris(dimethylaminomethyl)phenol, were added to the mixture and stirred until a homogeneous dispersion was obtained. Thereafter, the resulting solution was poured into a Teflon mold and was degassed for 30 min. It was then cured at 230°C for 30 min in air. The resulting epoxy nanocomposites were removed on cooling and polished using 120 grit SiC paper before the DMA and TMA testing.

RESULTS AND DISCUSSION

Synthesis and Characterization of PAPPS

Bassindale et al.[34] synthesized T_8 from trialkoxysilanes in 20–95% yields in the presence of TBAF solution containing 5% water, and found that the fluoride ion plays an important role in forming the Si—O—Si framework with no reaction occurring if tetrabutylammonium chloride is used instead. Moreover, silanol groups (RSiOH) likely form as intermediates during the reaction. Asuncion and Laine[39] prepared T_{10} and T_{12} from T_8 using TBAF catalyst anticipating that the mechanism begins with the cleavage of Si—O—Si bonds by the strong nucleophilic fluoride ion or hydroxide ion to form $RSiO_2^-$ fragments followed by reassembling to larger cages.

Cage rearrangements were explored by Rikowski and Marsmann[44] in 1997 in efforts to prepare T_{10} and T_{12} from related T_8 SQs using various bases in acetone and acetonitrile. Recently, Laine et al.[18,39,40] described fluoride-mediated rearrangement of T_8 SQs in THF at room temperature using TBAF catalyst to produce mixtures of di- and trifunctional T_{10} and T_{12} (R = phenyl, vinyl and methyl) in 80–90% yields using random-structured SQs as starting materials.

Even though TBAF was found to be a suitable catalyst for the generation of the T_{10} and T_{12} cages, solvent removal resulted in repolymerization of products to form undesired high MW polymers took place if the fluoride ion was retained in the reaction mixture. Thus, calcium chloride ($CaCl_2$) was used to trap excess

Applied Polymer SCIENCE

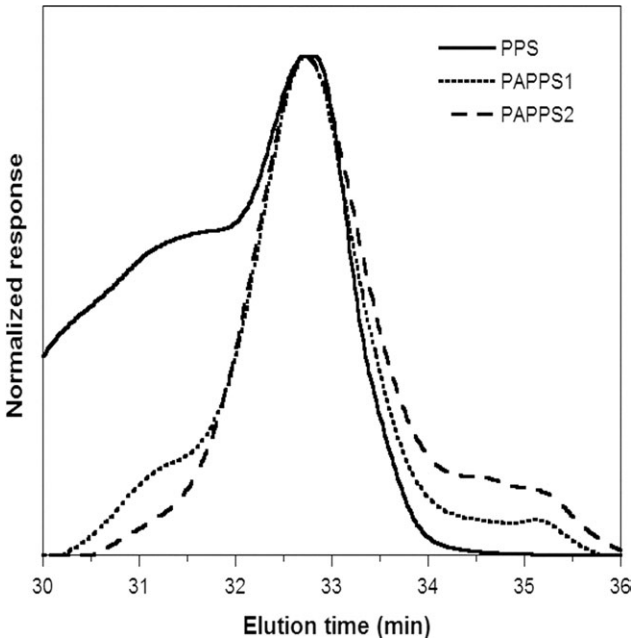

Figure 1. GPC analyses on PPS, PAPPS1, and PAPPS2.

fluoride ion forming insoluble calcium fluoride salt (CaF_2) and insoluble tBu_4NCl which are removed easily by filtration.[40]

GPC analyses of PPS, PAPPS1, and PAPPS2 after workup (5 mol % TBAF, room temperature, 4 days) are displayed in Figure 1. PPS does not completely dissolve in THF; however, GPC data of soluble PPS is composed of a sharp peak at ca. 32.8 min (Mp = 895) with a broad shoulder in the 30.7–32.0 min range. The broad shoulder changes into a narrow peak at ca. 32.5 min, indicating that the reaction is complete and most of the high MW polymer has transformed into low MW species during the reaction. PAPPS1 and PAPPS2 exhibit very similar elution times that can be associated with the spherical nature of the products rather than reflecting the different molecular weights of the T_{10} and T_{12} components as seen elsewhere.[18] In addition, the absence of any shoulders at shorter retention times suggests that the starting PPS has been mostly consumed.

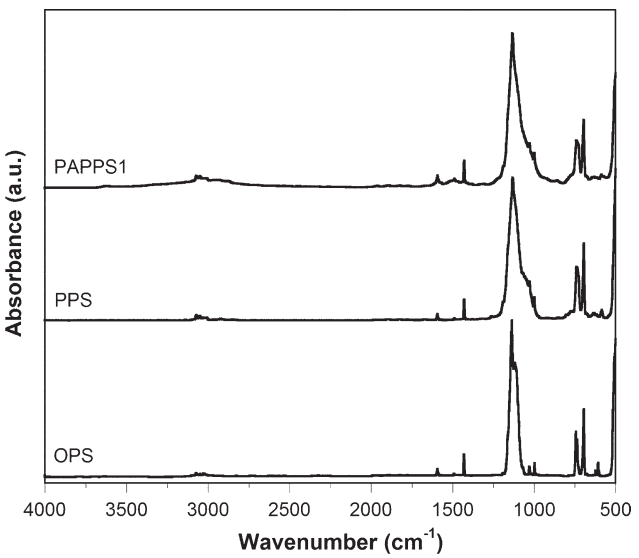

Figure 2. FTIR spectra on the OPS, PPS, and PAPPS1.

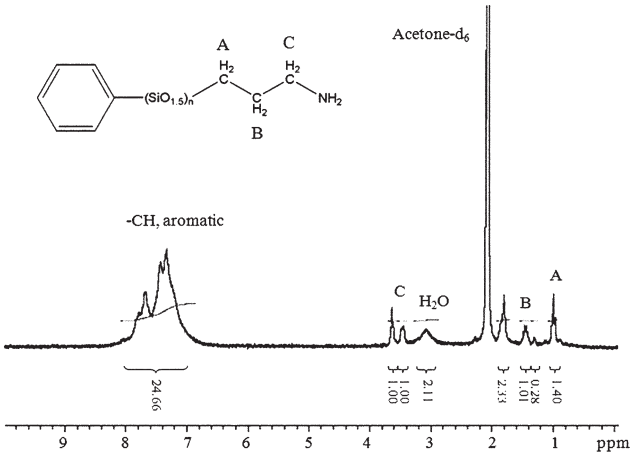

Figure 3. ^{1}H-NMR spectrum on the PAPPS1.

Figure 2 compares the FTIR spectrum of octa(phenyl)SQ (OPS) with those of the starting PPS and PAPPS1 (spectrum of PAPPS2 is similar to that of PAPPS1). Previous work[19] reported that T_8, T_{10}, and T_{12} SQs exhibit a sharp singlet for a symmetric Si—O—Si stretching vibration in a range of 1120–1130 cm^{-1}, whereas polymeric SQs exhibit two bands at 1135–1150 and 1045–1060 cm^{-1} which are characteristic of *v*Si—O—Si bands of cages, and those of partial cages, respectively. Hence, PAPPS1, which shows an FTIR spectrum similar to that of PPS presumably also consists of cages and partial cages structures. Furthermore, a medium peak at 1400–1600 cm^{-1} is associated with aromatic *v*C=C.

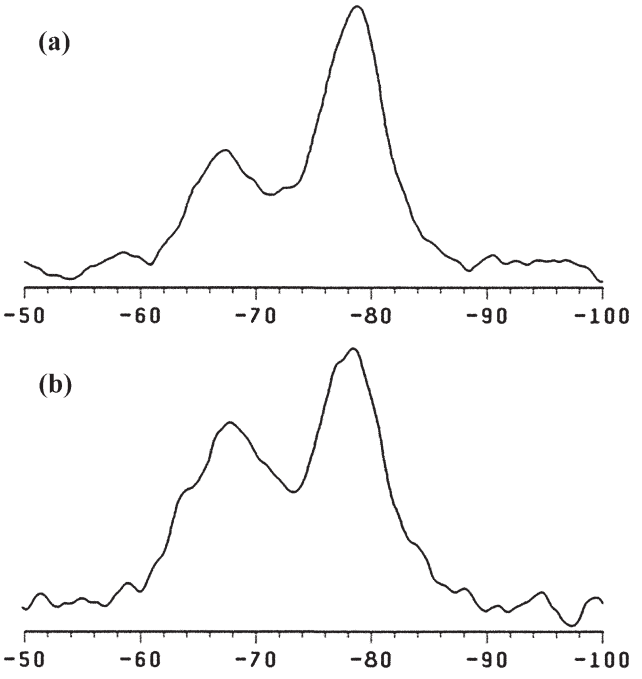

Figure 4. Solid-state ^{29}Si-NMR spectra on the (a) PAPPS1 and (b) PAPPS2.

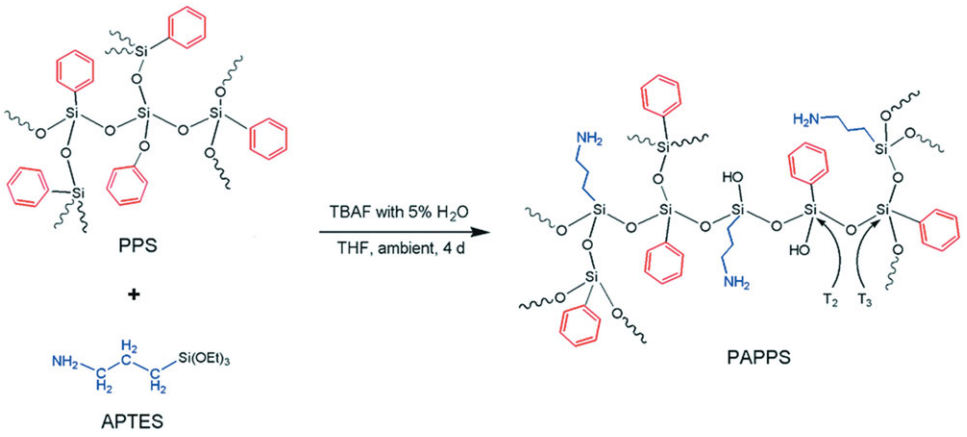

Scheme 2. Possible chemical structure of PAPPS. T_2 and T_3 design the doubly and completely condensed silicons.[Color figure can be viewed in the online issue, which is available at wileyonlinelibrary.com.]

As illustrated in Figure 3, the ^{1}H-NMR spectrum of PAPPS1 in acetone-d_6 (2.05 ppm; water in acetone-d_6 appears at 2.8 ppm) reveals the expected aromatic protons in the 7.00–8.00 ppm range. The exact chemical shift of —NH_2 is difficult to identify precisely because it depends on solvent used, temperature and concentrations. However, peaks with chemical shifts at 0.98 (A), 1.40 (B), and 3.45 (C) ppm can be assigned to protons on methylene groups (—CH_2—). Figure 4 shows the solid-state ^{29}Si-NMR spectra of PAPPS1 and PAPPS2. According to Frye et al.,[45] T_8 and T_{10} present singlets each related to the strain-free structures, while T_{12} shows two singlets suggesting its unstrained geometrical isomers. The ^{29}Si-NMR data of PAPPS1 and PAPPS2 display two broad peaks at ca. −67.5 and −78.4 ppm assigned to the T_3 and T_2 molecules, respectively.[46] These spectroscopic results correspond to the above-mentioned FTIR data. In accordance with FTIR, ^{1}H and solid state ^{29}Si-NMR data, the possible chemical structure of PAPPS is illustrated in Scheme 2.

The amino contents and thermal stabilities of PAPPS1 and PAPPS2 are listed in Table I. It shows that PAPPS2 exhibits a higher amine content compared to that of PAPPS1, which corresponds to the molar ratio of PPS/APTES, resulting in lower 5 and 20% mass loss temperatures because of the decomposition of aminopropyl chains. In contrast, PAPPS1 possesses higher mass loss temperatures owing to a larger number of highly stable aromatic rings. Ceramic yields indicate that the silica contents of PAPPS1 and PAPPS2 are almost identical.

Preparation and Characterization of Epoxy Nanocomposites

Table II presents the properties of epoxy nanocomposites for various reinforcing component type and loading, e.g., glass transition temperature (T_g), rubbery state modulus, decomposition temperature and char yield. Incorporating PAPPS1 and PAPPS2 into epoxy resins results in nanocomposites with better thermal stabilities than those of the neat epoxy because the silica introduces as the SQ cores and phenyl rings. In comparison with neat epoxy, the 5% mass loss temperatures of EC1-5 and EC2-5 increase by ~30° and 20°C. The char yields at 1000°C under nitrogen of EC1–5 and EC2–5 increase by 2.6 and 2.4 times, respectively. The epoxy nanocomposites containing PAPPS1 have slightly higher thermal stabilities than those of PAPPS2 for reasons described above.

Figure 5 displays the storage modulus (E'), loss modulus (E'') and tan δ for the neat epoxy. It shows a T_g at 85°C based on the maximum peak of tan δ peaks or at 73°C based on the maximum peak of the loss modulus. The magnitude of the storage modulus in the rubbery plateau region (T_g+40°C) is an indication of the crosslink densities of the nanocomposites with an increase in the storage modulus being due to greater degree of crosslinking within the system. The T_g of epoxy nanocomposites based on the maximum peak of tan δ increases with increasing SQ loading as shown in Figure 6. EC1–5 gives the highest T_g of 106 ± 5°C. The single peak of tan δ reveals that the epoxy nanocomposites were homogeneous.

Coefficients of thermal expansion (CTEs) below the T_g of epoxy nanocomposites gradually decrease with increasing in SQ loading as demonstrated in Figure 7. Neat epoxy has a CTE of 80 ppm/°C.[47] Introduction of PAPPS1 (PAPPS2) restricts polymer segment movement due to direct coupling with DGEBA to form a nanocomposite with higher crosslink densities thereby

Table I. Amino Functional Group Content and TG/DTA Results for PAPPS1 and PAPPS2

Sample	Molar ratios of PPS: APTES	Amino content[a] (mmol-NH_2)	Elemental analysis (%)			T_d (5%)[b] (°C)	T_d (20%)[c] (°C)	CY[d] (%)
			C	H	N			
PAPPS1	1 : 1.5	0.18	42.56	4.71	1.35	286	476	45.5
PAPPS2	1 : 5.0	0.45	34.71	5.50	1.57	244	422	44.5

[a]Determined by back titration, [b]T_d (5%): 5% mass loss temperature under air, [c]T_d (20%): 20% mass loss temperature under air, [d]CY, ceramic yield at 1000°C under air.

Table II. The Properties of Nanocomposites from PAPPS1 and PAPPS2

Sample	Filler type	Wt % filler	T_g (°C)[a]	Rubbery state modulus (MPa)[b]	T_d (5%)[c] (°C)	Char yield[d] (%)	CTE[e] (ppm/°C)
Neat epoxy	–	0	85	2.03	328	4.66	80
EC1-1	PAPPS1	1	88	2.62	344	7.61	75
EC1-3	PAPPS1	3	99	3.41	352	9.16	72
EC1-5	PAPPS1	5	106	4.20	356	12.14	67
EC2-1	PAPPS2	1	92	2.86	339	7.24	70
EC2-3	PAPPS2	3	97	3.95	350	9.18	66
EC2-5	PAPPS2	5	106	5.15	349	11.43	63

[a]Determined from maximum peak of tan δ, [b]Determined at T_g+40°C, [c]T_d (5%): 5% mass loss temperature under nitrogen (°C), [d]Char yield at 1000°C under nitrogen, [e]CTE (ppm/°C) was collected below infection point of TMA plot.

reducing the CTE. The epoxy nanocomposites from PAPPS2 exhibit lower CTEs than those from PAPPS1 because of greater number of aminopropyl chains as evidenced by back titration and elemental analysis in Table I. The crosslink density of epoxy nanocomposites indicated by the storage modulus in the rubbery plateau as shown in Table II confirms this result. EC1–5 and EC2–5 have CTEs of 67 ppm/°C and 63 ppm/°C, which are 16 and 21% lower than that of neat epoxy.

Furthermore, we concluded that an increase of crosslink density is the major factor affecting the thermomechanical properties of composites, i.e., CTE and T_g, compared with the reinforcing effect. According to TGA data of PAPPS1 and PAPPS2 shown in Table I the ceramic yields, which imply the inorganic content, of PAPPS1 and PAPPS2 are nearly identical indicating that at the same filler content the reinforcing effect of PAPPS1 and PAPPS2 on the thermomechanical properties of composites should be almost identical too. Additionally, the crosslink density of composites contained PAPPS2 is higher than that contained PAPPS1 as confirmed by the higher storage modulus in rubbery plateau, which implies the crosslink density of composites, as displayed in Table II.

CONCLUSIONS

The poly(aminopropyl/phenyl)SQs were not only synthesized from PPS and APTES at different molar ratios (PAPPS1 and PAPPS2) in THF solvent with TBAF catalyst containing scarce water, but also used as organic/inorganic components for improvement of thermomechanical properties of epoxy nanocomposites. FTIR, ^{1}H, solid-state ^{29}Si-NMR studies of both PAPPS1 and PAPPS2 suggest that they likely consist of cages and possibly some partial cages containing both aminopropyl and phenyl functionalized SQs. PAPPS1 offers a greater number of phenyl rings than PAPPS2 as proved by back titration and

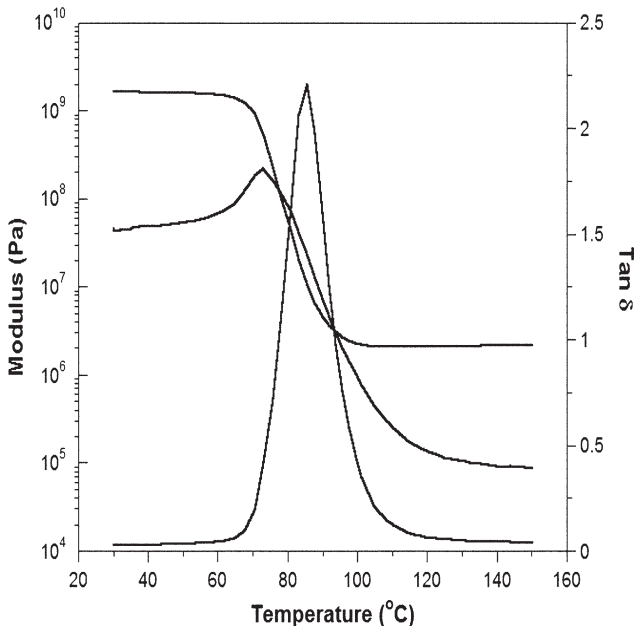

Figure 5. Thermomechanical plots for neat epoxy at a heating rate of 5°C/min.

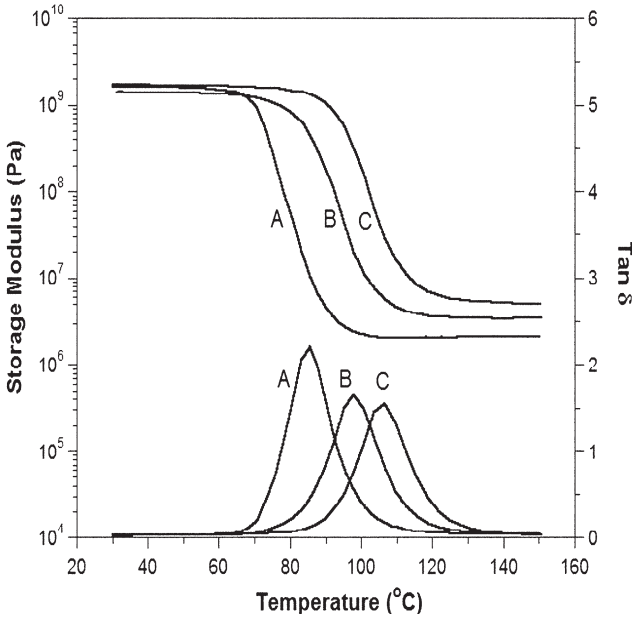

Figure 6. Thermomechanical profiles of: (A) neat epoxy, and epoxy nanocomposites containing PAPPS1 at (B) 1 wt % and (C) 5 wt % at a heating rate of 5°C/min.

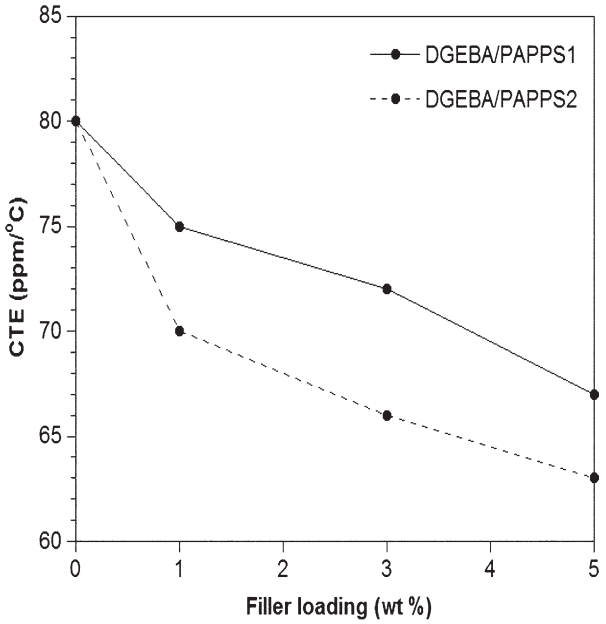

Figure 7. Coefficients of thermal expansion (CTEs) of epoxy nanocomposites filled with PAPPS1 and PAPPS2 at different filler loadings.

elemental analysis. In comparison with neat epoxy, incorporating these fillers can improve the properties of nanocomposites. Epoxy nanocomposites filled with PAPPS1 show superior thermal stabilities, whereas epoxy nanocomposites filled with PAPPS2 show lower CTEs.

The authors would like to thank Chulalongkorn University 100th Anniversary grant and Rachadapiseksompoch grant for financial support of this work. C. S. would like to thank Mr. Jae Hwan Jung for recording all the ^{1}H-NMR data. Researchers at UM would like to thank Boeing Co. for partial support of this work.

REFERENCES

1. Abeand, Y.; Gunji, T. *Prog. Polym. Sci.* **2004**, *29*, 149.
2. Baney, R. H.; Itoh, M.; Sakakibara, A.; Suzuki, T. *Chem. Rev.* **1995**, *95*, 1409.
3. Calzaferri, G. In Taylor-made Silicon-Oxygen Compounds, from Molecules to Materials; Corriuand, R.; Jutzi, P., Eds.; Vieweg mbH: Wiesbaden, **1996**, p 149.
4. Chan, K. L.; Sonarand, P.; Sellinger, A. *J. Mater. Chem.* **2009**, *19*, 9103.
5. Cordes, D. B.; Lickissand, P. D.; Rataboul, F. *Chem. Rev.* **2010**, *110*, 2081.
6. Duchateau, R. *Chem. Rev.* **2002**, *102*, 3525.
7. Kannan, R. Y.; Salacinski, H. J.; Butlerand, P. E.; Seifalian, A. M. *Acc. Chem. Res.* **2005**, *38*, 879.
8. Laine, R. M. *J. Mater. Chem.* **2005**, *15*, 3725.
9. Laineand, R. M.; Roll, M. F. *Macromolecules* **2011**, *44*, 1073.
10. Li, G. Z.; Wang, L. C.; Niand, H. L.; Pittman, C. U. *J. Inorgan. Organometal. Polym.* **2001**, *11*, 123.
11. Lichtenhan, J. D. In Polymeric Materials Encyclopedia; Salamone, J. C., Ed.; CRC Press: New York, **1996**, p 7769.
12. Lickissand, P. D.; Rataboul, F. *Adv. Organometallic Chem.* **2008**, *57*, 1.
13. Loyand, D. A.; Shea, K. *J. Chem. Rev.* **1995**, *95*, 1431.
14. Phillips, S. H.; Haddadand, T. S.; Tomczak, S. *J. Curr. Opin. Solid State Mater. Sci.* **2004**, *8*, 21.
15. Provatasand, A.; Matisons, J. G. *Trends Polym. Sci.* **1997**, *5*, 327.
16. Voronkovand, M. G.; Lavrent'yev, V. I. *Top. Curr. Chem.* **1982**, *102*, 199.
17. Wuand, J.; Mather, P. T. *Polym. Rev.* **2009**, *49*, 25.
18. Jungand, J. H.; Laine, R. M. *Macromolecules* **2011**, *44*, 7263.
19. Brown, J. F.; Vogtand, L. H.; Prescott, P. I. *J. Am. Chem. Soc.* **1964**, *86*, 1120.
20. Zhang, C.; Babonneau, F.; Bonhomme, C.; Laine, R. M.; Soles, C. L.; Hristovand, H. A.; Yee, A. F. *J. Am. Chem. Soc.* **1998**, *120*, 8380.
21. Choi, J.; Tamaki, R.; Kimand, S. G.; Laine, R. M. *Chem. Mater.* **2003**, *15*, 3365.
22. Huang, J. C.; He, C. B.; Xiao, Y.; Mya, K. Y.; Daiand, J.; Siow, Y. P. *Polymer* **2003**, *44*, 4491.
23. Kim, S. G.; Choi, J. ; Tamakiand, R. ; Laine, R. M. *Polymer* **2005**, *46*, 4515.
24. Ni, Y.; Zhengand, Z.; Nie, K. *Polymer* **2004**, *45*, 5557.
25. Takahashi, K.; Sulaiman, S.; Katzenstein, J. M.; Snoblenand, S.; Laine, R. M. *Aust. J. Chem.* **2006**, *59*, 564.
26. Choi, J.; Harcup, J.; Yee, A. F.; Zhuand, Q.; Laine, R. M. *J. Am. Chem. Soc.* **2001**, *123*, 11420.
27. Choi, J. ; Yeeand, A. F. ; Laine, R. M. *Macromolcules* **2003**, *36*, 5666.
28. Huang, J.; Xiao, Y.; Mya, K. Y.; Liu, X.; He, C.; Daiand, J.; Siow, Y. P. *J. Mater. Chem.* **2004**, *14*, 2858.
29. Leeand, L. H.; Chen, W. C. *Polymer* **2005**, *46*, 2163.
30. Brick, C. M.; Ouchi, Y.; Chujoand, Y.; Laine, R. M. *Macromolcules* **2005**, *38*, 4661.
31. Roll, M. F.; Asuncion, M. Z.; Kampfand, J.; Laine, R. M. *ACS Nano* **2007**, *2*, 320.
32. Sprungand, M. M.; Guenther, F. O. *J. Am. Chem. Soc.* **1955**, *77*, 3996.
33. Sprungand, M. M.; Guenther, F. O. *J. Am. Chem. Soc.* **1955**, *77*, 3990.
34. Bassindale, A. R.; Liu, Z.; MacKinnon, I. A.; Taylor, P. G.; Yang, Y.; Light, M. E.; Hortonand, P. N.; Hursthouse, M. B. *Dalton Trans.* **2003**, *14*, 2945.
35. Liu, Z.; Bassindaleand, A. R.; Taylor, P. G. *Chem. Res. Chinese U.* **2004**, *20*, 433.
36. Koželjand, M.; Orel, B. *Dalton Trans.* **2008**, *37*, 5072.
37. Bassindale, A. R.; Parker, D. J.; Pourney, M.; Taylor, P. G.; Hortonand, P. N.; Hursthouse, M. B. *Organometallics* **2004**, *23*, 4400.
38. Anderson, S. E.; Bodzin, D. J.; Haddad, T. S.; Boatz, J. A.; Mabry, J. M.; Mitchelland, C.; Bowers, M. T. *Chem. Mater.* **2008**, *20*, 4299.

39. Asuncionand, M. Z.; Laine, R. M. *J. Am. Chem. Soc.* **2010**, *132*, 3723.
40. Ronchi, M.; Sulaiman, S.; Bostonand, N. R.; Laine, R. M. *Appl. Organometal. Chem.* **2010**, *24*, 551.
41. Kim, S. G.; Sulaiman, S.; Fargierand, D.; Laine, R. M. In Materials Syntheses: A Practical Guide; Schubert, U.; Hüsingand, N.; Laine, R. M., Eds.; Springer: New York, **2008**, p 179.
42. Liu, S.; Lang, X.; Ye, H.; Zhangand, S.; Zhao, J. *Eur. Polym. J.* **2005**, *41*, 996.
43. Tsubokawa, N.; Iidaand, T.; Takayama, T. *J. App. Polym. Sci.* **2000**, *75*, 515..
44. Rikowskiand, E.; Marsmann, H. C. *Polyhedron* **1997**, *16*, 3357.
45. Fryeand, C. L.; Collins, W. T. *J. Am. Chem. Soc.* **1970**, *92*, 5586.
46. Prado, L. A. S. D. A.; Radovanovic, E.; Pastore, H. O.; Yoshidaand, I. V. P.; Torriani, I. L. *J. Polym. Sci. Part A: Polym. Chem.* **2000**, *38*, 1580.
47. Suwanchatchai, K.; Somwangthanaroj, A. *Submitted* (**2012**).